

Communications

Dual Band-Reject UWB Antenna With Sharp Rejection of Narrow and Closely-Spaced Bands

Ahmad A. Gheethan and Dimitris E. Anagnostou

Abstract—An ultrawideband (UWB) antenna that rejects extremely sharply the two narrow and closely-spaced U.S. WLAN 802.11a bands is presented. The antenna is designed on a single surface (it is uniplanar) and uses only linear sections for easy scaling and fine-tuning. Distributed-element and lumped-element equivalent circuit models of this dual band-reject UWB antenna are presented and used to support the explanation of the physical principles of operation of the dual band-rejection mechanism thoroughly. The circuits are evaluated by comparing with the response of the presented UWB antenna that has very high selectivity and achieves dual-frequency rejection of the WLAN 5.25 GHz and 5.775 GHz bands, while it receives signal from the intermediate band between 5.35–5.725 GHz. The rejection is achieved using double open-circuited stubs, which is uncommon and are chosen based on their narrowband performance. The antenna was fabricated on a single side of a thin, flexible, LCP substrate. The measured achieved rejection is the best reported for a dual-band reject antenna with so closely-spaced rejected bands. The measured group delay of the antenna validates its suitability for UWB links. Such antennas improve both UWB and WLAN communication links at practically zero cost.

Index Terms—Dual-band-reject, equivalent circuits, ultrawideband (UWB), WLAN.

I. INTRODUCTION

Although the 2.4–2.835 GHz WLAN band is outside the 3.1–10.6 GHz ultrawideband (UWB) spectrum [1], WLAN systems in the United States function also on 12 more channels: eight for the ‘lower and middle’ band $R_1 = 5.15 - 5.35$ GHz, and four for the ‘upper, outdoor band’ $R_2 = 5.725 - 5.825$ GHz [2]. Therefore, a UWB antenna that receives typically a few nanowatts from a UWB signal will also receive interfering signal from coexisting WLAN devices intercommunicating at 5.15–5.875 GHz. To suppress this interference, researchers have developed various band-notched UWB designs that reject typically the 5.15–5.875 GHz WLAN band or a large part of it. Characteristic examples include (but are not limited to) [3]–[6]. However results show that the filtering cannot be achieved with the same rejection level in the entire WLAN band. An additional challenge is that the required frequencies to be rejected are only R_1

Manuscript received August 02, 2010; revised April 03, 2011; accepted April 07, 2011. Date of publication January 31, 2012; date of current version April 06, 2012. This material is based upon work supported in part by the Defense Advanced Research Projects Agency (DARPA)/Microsystems Technology Office (MTO) Young Faculty Award program under Award No. N66001-11-1-4145, by the US Army Research Laboratory/Army Research Office under agreement number W911NF-09-1-0277, the National Science Foundation under agreements ECS-0824034 and EPS-0903804, and in part by the NASA under Cooperative Agreement NNX07AL04A..

D. E. Anagnostou is with the South Dakota School of Mines and Technology, Rapid City, SD 57701 USA and also with Democritus University of Thrace, Xanthi 67100, Greece (e-mail: danagn@ieee.org).

A. A. Gheethan was with the South Dakota School of Mines and Technology, Rapid City, SD 57701 USA. He is now with the University of South Florida, Tampa, FL 33620 USA.

Color versions of one or more of the figures in this communication are available online at <http://ieeexplore.ieee.org>.

Digital Object Identifier 10.1109/TAP.2012.2186221

and R_2 with extremely narrow bandwidths of 0.2 GHz and 0.1 GHz respectively, but most antennas reject also the intermediate band $R_{int} = 5.35 - 5.725$ GHz.

If a UWB receiver could reject each individual WLAN band only, it would be capable of receiving the intermediate R_{int} band signal. In addition, if the UWB transmitter could achieve the same rejection, its signal would interfere less with WLAN receivers and that could be important in cases where the received WLAN signal is weak. Therefore the design and comprehension of efficient band-rejection mechanisms is important to the antenna engineer as their implementation can lead to increased S/N ratios for both the UWB and the WLAN links and provide devices that are more power efficient.

Various band-reject UWB antenna designs exist. Their majority uses slots and some have widely-separated rejection bands (e.g., [7]) or reject the entire 5.15–5.825 GHz band and thus suppress also the 5.35–5.725 GHz signal (which this antenna is designed to accept) (e.g., [8]). Recent literature shows UWB designs with dual and triple band cutoffs. In [9], a dual-notched design was discussed by Ryu *et al.* using parametric studies. The design has high rejection level in R_1 but not as high in R_2 where the VSWR is 4 and the antenna gain is over -1.5 dBi. A triple notch was achieved with Ω -shaped slots and additional slits on its (defective) ground plane by Li *et al.* in [10]. The design exhibits a sharp simulated rejection response; however, it is complicated and hard to replicate, fine-tune and scale due to the required backside etching and to the curvature of the slots. Etching accurately fine features on the backside of a substrate often requires backside mask alignment, which is difficult on opaque substrates and causes delays, adds to the cost, and is a major source of inaccuracies in prototyping labs. Also existing uniplanar band-reject antennas differ by having widely separated rejected bands, using slots and/or having single-band rejection.

In this work, the first uniplanar UWB antenna design that achieves the rejection of two extremely narrow and closely-spaced frequencies is presented. This communication extends the dual-slot approach by Anagnostou *et al.* [11], to a linear open-circuited double stub that *a*) is simple to design, *b*) achieves significantly sharper rejection characteristic than slots and *c*) is easy to fine-tune because it consists only of linear sections for the stubs and antenna, making it an easy task to maintain constant the distance of the stubs from the antenna edges. Its straight edges make it constructible using any of the 4 basic technologies (photolithography/etching, milling, direct-write printing, screen printing) without needing any additional processing (vias, wire-bonds, etc.). Curves, for example, often result to inaccuracies when printed using direct-write techniques. A conformal octagonal-shaped UWB radiator is designed and two resonant stubs are added on each side to enable the rejection of both WLAN bands R_1 and R_2 with very sharp (high- Q) cutoff. This allows the antenna to receive the intermediate band R_{int} . Note that open-circuit stubs are rarely used because they reject narrow bands. Here we illustrate how they can be properly used to achieve the desired dual-band rejection.

For the design of such antennas it is important to comprehend the operation of the band-rejection mechanism of the stubs and radiating element. We provide a physical explanation of the rejection mechanism, supported by a distributed-element equivalent circuit and a lumped-element equivalent circuit models that are developed. The simulated results are validated with measurements. The distributed equivalent circuit provides a physical interpretation of the rejection mechanism by

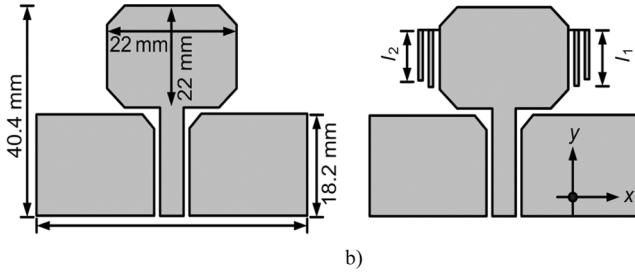


Fig. 1. Schematic of the UWB antennas: (a) traditional design without notched response, and (b) dual-notched response design.

studying the current on the antenna. The lumped equivalent circuit had been used so far only to describe the multiple resonances of the impedance of UWB antennas. Here it is used to prove our hypothesis that very sharp rejections can be achieved with high- Q resonators, and to calculate the Q -factor of these resonators. Thus it also helps illustrate the rejection properties of the UWB antenna and to understand how its input impedance will be affected by the added inductance and capacitance from the stubs, which can be used to accelerate large system simulations. The comprehension of the rejection mechanism is also assisted by the illustrations and explanations of the current on the structure. It is important as it can help engineers fine-tune designs faster by applying critical thinking and thus reducing the full wave computational effort.

A prototype was fabricated on thin, lightweight liquid crystal polymer (LCP) substrate and was measured to validate the reliability of the simulated results. The measured results for the gain, radiation patterns and group delay are presented and discussed. The measured response is the best reported of its kind (dual and narrow-band rejection).

The presented design methodology and band-reject mechanism principles of operation are generalized and can be applied to all uniplanar dual-band reject UWB antennas and even to some dual-layer designs. It can also easily be extended to multi-band reject antennas. Furthermore, it can be used with other antenna structures in planar and/or volumetric configuration (e.g., rectangular, circular, elliptical, spherical, oval), regardless of their feed mechanism.

II. ANTENNA DESIGN AND EQUIVALENT CIRCUIT MODELS

A. Antenna Design

Fig. 1 shows schematics of the proposed UWB antenna with and without band-reject characteristic. The antenna is octagonal-based and made on 0.1016 mm thick and flexible LCP substrate with a relative permittivity $\epsilon_r = 3.1$ and dielectric loss tangent $\tan \delta = 0.0019$. It is fed using a 50 Ω coplanar waveguide (CPW) line. Its operation can be interpreted with a wideband transition from a CPW line to two parallel slot lines of tapered characteristic impedance that are formed between the radiating element and ground planes of the CPW line (Fig. 1(a)). Both slot lines transform 377 Ω to a parallel combination of two 100 Ω loads resulting in a 50 Ω load connected to the CPW line. This transition provides the wideband matching for the antenna. Also, two small triangular slots are made at the feed point to increase the input capacitance at higher frequencies for matching purposes.

To achieve the dual cutoff, two stubs are added on each side of the antenna (Fig. 1(b)). The longer stub should be located close to the antenna and have length l_1 equal to $\lambda_g/4$ at 5.25 GHz, while the second (l_2) is shorter and is $\lambda_g/4$ long at 5.775 GHz. The guide wavelength (λ_g) is defined as:

$$\lambda_g = \frac{c}{\sqrt{\epsilon_{\text{eff}} f}} \quad (1)$$

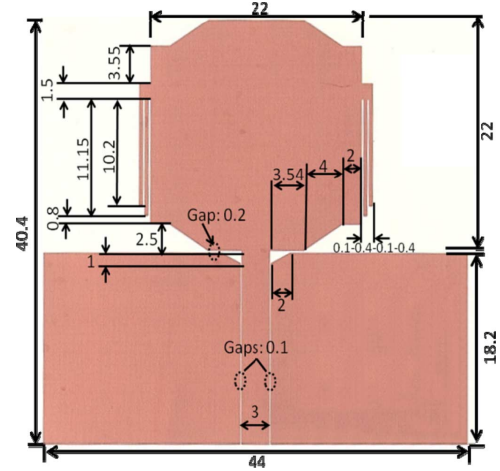


Fig. 2. Photo of the double-notched UWB antenna fabricated on LCP. All dimensions are [mm]. The traditional design is similar but without the stubs.

where c is the free-space speed of light, f the center of the desired notch frequency, and ϵ_{eff} the effective relative permittivity. The latter parameter is of interest: as it will be shown later, the stubs form a coplanar strip (CPS) transmission line with their respective adjacent conductor of the structure. Therefore the CPS design equations were used to calculate the effective dielectric constant of the structure and find the initial stubs lengths [12]. This is important since the antenna is CPW-fed and the use of CPW line design equations for the stubs would lead to erroneous results. Using MatLAB, it was calculated that $\epsilon_{\text{eff}} = 1.37$ and from (1) the initial lengths l_1 and l_2 were also calculated $l_1 = 12.25$ mm and $l_2 = 11.13$ mm, and were later fine-tuned to $l_1 = 12.65$ mm and $l_2 = 11.7$ mm using simulations. The stubs were chosen to be 0.4 mm wide and their separation gap only 0.1 mm. Fig. 2 shows a photo of the fabricated antenna before soldering the SMA connector, with its design dimensions superimposed.

The rejection mechanism is analyzed next. Strong rejection is achieved when adjacent currents flow in opposite directions (transmission-line mode, TL) and cancel the radiated fields. This is facilitated here by using linear stubs and antenna sections that maintain a constant separation distance. At the notch frequencies, the current flowing on the stubs is in opposite direction (out-of-phase) from the current on the antenna edges. This makes the antenna and stubs function in the TL mode and the strongest rejection occurs when the opposite components of the current density are also equal in amplitude. Figs. 3(a) and 5(a) show the simulated average vector current distribution on the antenna at 5.25 GHz. The current flow on the non-resonant Stub2 is small and Stub1 cancels the radiation from the antenna, resulting in R_1 being rejected. Figs. 3(b) and 5(b) show the 5.775 GHz distribution. Here little current exists on the actual antenna edge because the open-circuited Stub1 draws more current by presenting low impedance at its anchor. Thus, Stub1 acts as the edge of the antenna, and its radiation is cancelled by the out-of-phase current in Stub2. The current distribution at 4 GHz, 7 GHz, and 10 GHz is also shown in Fig. 3(c)–(e). The current flows mostly on the perimeter and is strong at the bottom and side edges while it becomes insignificant at the top. It is symmetric on the left and right sides as expected due to structural symmetry and is very small along the stubs. At the lower frequencies (~ 4 GHz), radiation originates from the entire structure (current flows mainly around the edges). At higher frequencies (above ~ 6 GHz) radiation originates mainly from the tapered planar TEM horns on the lower edge of the antenna.

This antenna was fabricated and its measured VSWR in Fig. 4 shows that dual-frequency cutoff is clearly achieved with VSWR of 6.73 (at

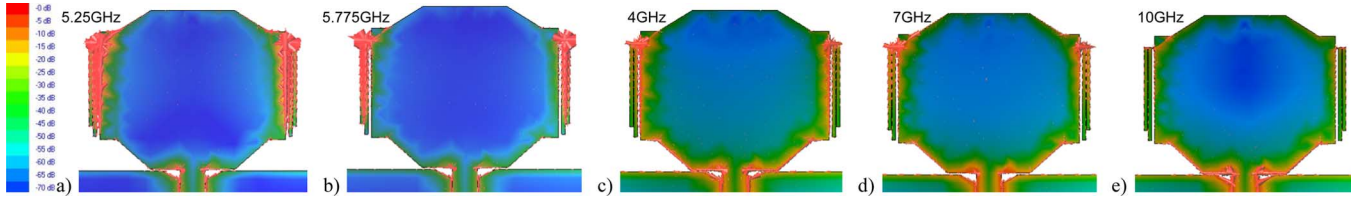


Fig. 3. Simulated average vector current distribution over the UWB design at various frequencies. The current density is high on the stubs at the resonant frequencies 5.25 GHz and 5.775 GHz, while it is low at the other frequencies.

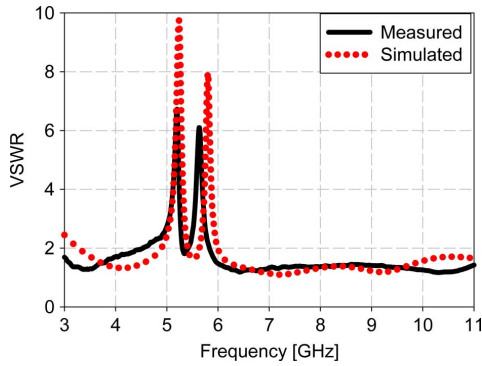


Fig. 4. Simulated and measured VSWR of the dual-notched UWB antenna.

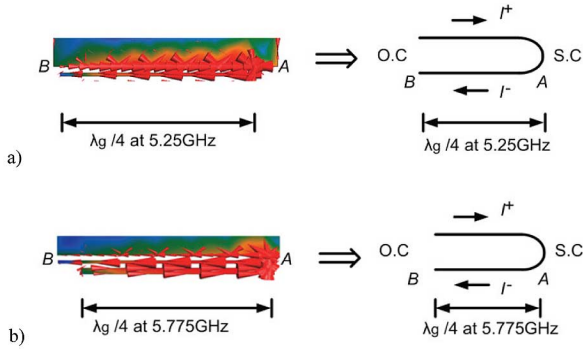


Fig. 5. Modeling of the antenna edge and stubs: (a) 5.25 GHz, note the very little current on the second (small/lower) stub, (b) 5.775 GHz.

5.22 GHz) and 6.1 (at 5.7 GHz). The slight shift between the measured and simulated cutoff frequencies is due to fabrication inaccuracies (e.g., over-etching) and uncertainties in the substrate effective permittivity which usually has to be estimated experimentally. However since substrate materials may vary amongst manufacturers, the design methodology and proof of concept are the main foci of this work.

B. Distributed Element Equivalent Circuit Model

The distributed model provides a physical interpretation of the rejection mechanism. As mentioned earlier, the antenna is in TL mode at the frequencies where out-of-phase currents flow along its edges and adjacent stubs. Then, its input impedance (Z_{in}) response can be accurately approximated by an equivalent distributed element circuit with open-and/or short-circuited stubs in series or parallel configuration based on the current distribution on the antenna [13].

The current on the antenna’s edge (I^+) at 5.25 GHz is equal in amplitude and out of phase with the current on Stub1 (I^-), as shown in Fig. 5(a). The current has high density at point A and low density at point B. Consequently, the antenna’s edge and Stub1 are modeled as a TL short-circuited at point A. The resultant equivalent load at point B is a high input-impedance open-circuit due to the TL length of $\lambda_g/4$ at 5.25 GHz. This open-circuit is transferred along the antenna structure

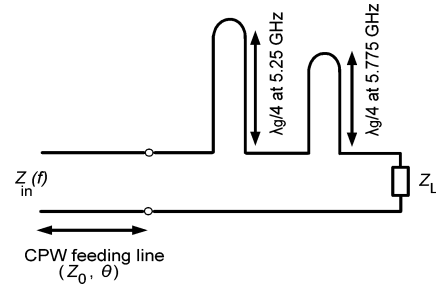


Fig. 6. Schematic of the equivalent distributed elements circuit of the dual band-reject UWB antenna.

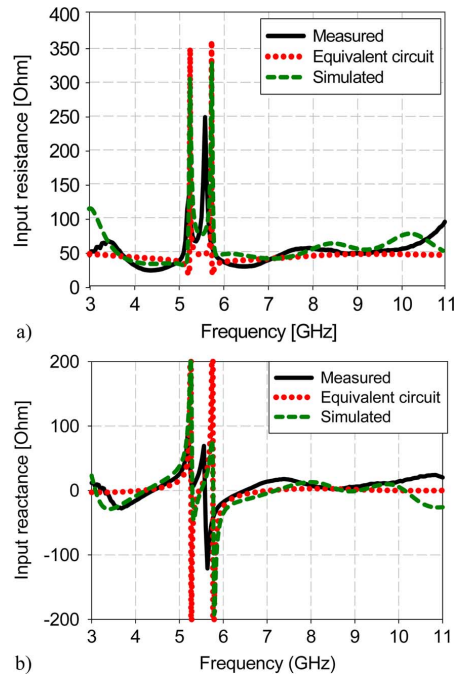


Fig. 7. Simulated and measured input impedance of the dual-notched UWB antenna: (a) input resistance, and (b) input reactance. At the rejected frequencies the input impedance is similar to that of an open circuit resonator.

and is also the impedance that is seen by the feed-point of the antenna (i.e., the SMA connector) at the rejected frequencies. Therefore the antenna at 5.25 GHz appears as an OC load at the CPW feed line input. Fig. 5(b) shows the respective circuit at the second cutoff frequency (5.775 GHz).

The described mechanism is valid at each rejected band and results in the antenna equivalent circuit shown in Fig. 6. At each cutoff frequency, the series short-circuited stub transforms to an open-circuit load connected in series with Z_L , resulting in an open circuit resonator at both bands. The final input impedance value $Z_{in}(f)$ is then determined by electrical length θ^o , which is approximately 160^o and 176^o at 5.25 GHz and 5.775 GHz, respectively. The measured input impedance is shown

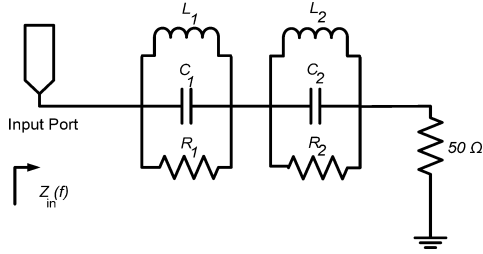


Fig. 8. Equivalent lumped-element circuit model of the dual band-reject UWB antenna.

TABLE I
CALCULATED VALUES OF THE EQUIVALENT CIRCUIT'S LUMPED ELEMENTS

Circuit	BW [MHz]	Q_0	R [Ω]	C [pF]	L [pH]
1	47	111.7	250	13.54	67.85
2	37	156.1	270	15.93	47.64

The distributed equivalent circuit response matches with the measured and simulated using IE3DTM.

in Fig. 7, compared with the results of the distributed equivalent circuit of Fig. 6 and of full-wave simulations carried out using IE3D.¹ The agreement of the results is apparent.

C. Lumped Element Equivalent Circuit Model

The antenna input impedance at the notch frequencies is similar to that of a lumped parallel RLC circuit. So, the proposed antenna can be modeled as a lumped-element circuit with two parallel RLC resonators connected in series with a 50Ω load as shown in Fig. 8. In that figure, the first parallel RLC resonates at 5.25 GHz and the second at 5.775 GHz, while the load approximates the radiation resistance of the antenna. The input resistance of the equivalent circuit at the rejected bands is maximum while its input reactance almost vanishes.

The lumped element equivalent circuit model illustrates the sharpness of the rejection mechanism by calculating the quality factor (Q_0) of the RLC resonators at the rejected bands. It also provides an accurate description for the input impedance response of the antenna through lumped entities that model the distributed elements. This description is easily comprehensible by engineers and scientists.

To complete this equivalent circuit, the values of the lumped elements need to be determined. To do so, the bandwidth BW and the quality factor Q_0 of the RLC resonators are needed. The RLC bandwidth is the range where the real part of the input impedance is equal to or greater than 0.707 of the maximum value. With the bandwidth known from the simulation results that are shown in Fig. 7(a), the Q_0 and lumped element values can be determined using [14]:

$$Q_0 = \frac{f_0}{\text{BW}} \quad (2)$$

$$Q_0 = 2\pi f_0 RC \quad (3)$$

$$f_0 = \frac{1}{2\pi\sqrt{LC}} \quad (4)$$

where f_0 is the resonant notch frequency and R , L and C the resistor, inductor and capacitor components of the RLC circuit respectively. The simulation was also used to determine the values of the resistors: 250Ω for the first RLC circuit and 270Ω for the second. The corresponding Q_0 and lumped element values were then calculated at 5.25 GHz and 5.775 GHz and are listed in Table I.

¹IE3D v.14, was a trademark of Zeland Corp., CA, 2009 and is now a trademark of Mentor Graphics, OR, 2012.

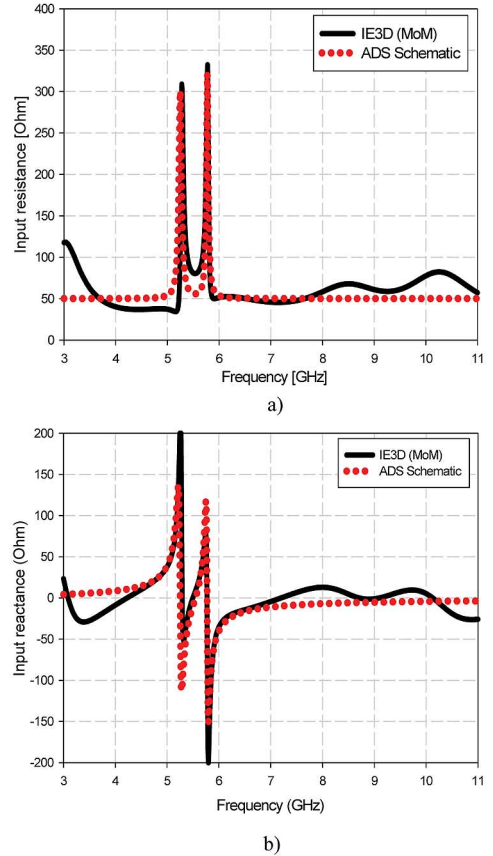


Fig. 9. (a) Input resistance, and (b) input reactance comparison for the dual-notched antenna using the full-wave simulator IE3D and the lumped-element equivalent circuit model response from ADS Schematic. The results are similar.

The lumped element equivalent circuit was also simulated in ADS Schematic environment² and the input impedance results are also included in Fig. 9 for comparison with the measurements and the full wave results from IE3D.

Although distributed models are often believed to be more accurate than lumped-element models, in this case both models provided very good accuracy. Here, the results from the lumped-element equivalent circuit model match well with those from the full-wave analysis over the entire UWB frequency range with little fluctuations.

III. ANTENNA DISPERSION, GAIN AND PATTERN RESULTS

To evaluate the suitability of the UWB antenna for UWB communication systems, it is necessary to measure its dispersion characteristics. To do so, the group delay was utilized, defined in the frequency domain as the first derivative of the far field phase of the transmission coefficient S_{21} with respect to the radial frequency ω [4]. The group delay was measured using two identical dual-stub UWB antennas facing each other and separated by a distance $d = 26$ cm, to allow far field conditions at all UWB frequencies. Measurements were carried out using an Agilent 8510C VNA, and were compared to simulations from IE3D.

The measured and simulated group delay is shown in Fig. 10(a) and is flat and low in the entire UWB range except at the rejected bands, as desired. Therefore the antenna is suitable for transmitting and receiving UWB pulses with minimum distortion, and thus can also be used in pulsed cognitive radio applications.

²Advanced Design System (ADS) v.2005A is a trademark of Agilent technologies.

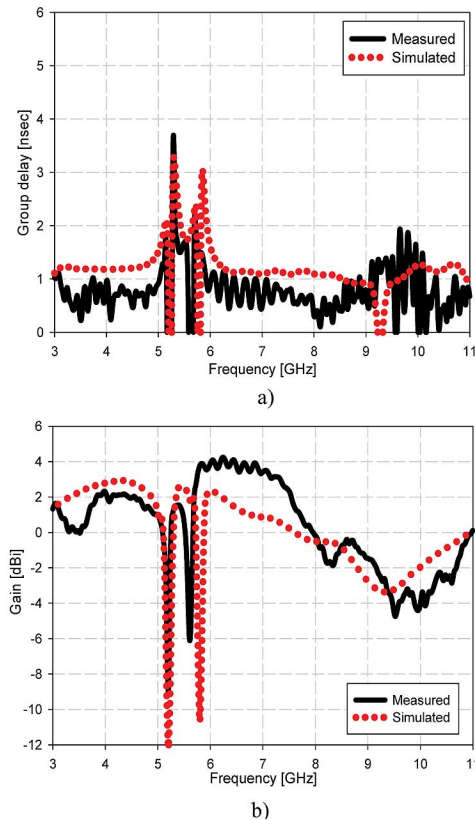


Fig. 10. Measured and simulated (IE3D) results of the dual-stubs antenna: (a) group delay, (b) broadside gain.

In addition, the broadside antenna gain was measured and is shown in Fig. 10(b). The gain was found to be lower than -8 dBi at 5.2 GHz and lower than -6 dBi at 5.65 GHz, so the measured achieved rejection is the best reported for a dual-band reject antenna with so closely-spaced rejected bands. It is also lower than the average gain of this design which was around $+2$ dBi.

The measured normalized radiation pattern in the E - and H - planes are shown in Fig. 11. The measurements were carried out at the custom built anechoic chamber of the South Dakota School of Mines and Technology. The toroidal-like pattern is almost omnidirectional at the measured frequencies in the H -plane, while it exhibits nulls in the E -plane. The patterns show little variation with frequency.

The antenna substrate is extremely flexible and a photo of the antenna under extreme flexing and with its SMA connector is shown in Fig. 12. The flexing radius was estimated approximately 0.5 cm but varied near the SMA due to its rigidity.

IV. DISCUSSION AND CONCLUSIONS

The first single-layer (uniplanar), dual band-reject UWB antenna that provides extremely sharp and closely-spaced rejected bands was presented and its distributed and lumped-element equivalent circuits were introduced. The challenging narrowband dual rejection was achieved with two resonant open-circuited stubs placed adjacent to the antenna edges that maximized the current cancellation and the suppression level of the rejected radiation at the desired frequencies.

The introduced distributed- and lumped-element equivalent circuits explain and help comprehend the functionality of the band-rejection mechanism. The circuits approximate accurately the input impedance of the antenna at all frequencies and their results are similar to the measurements and to the full-wave simulations.

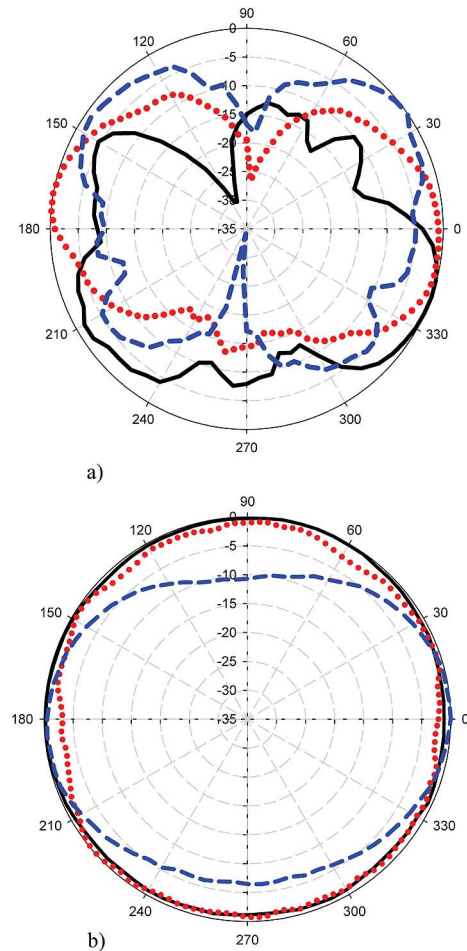


Fig. 11. Measured radiation pattern of the dual-notched antenna: (a) E -plane, and (b) H -plane. (Black solid line: 4 GHz, red dotted line: 7 GHz, blue dashed line: 10 GHz).



Fig. 12. Photo of the fabricated prototype under extreme flexing conditions.

The significance of this work is enhanced because the presented design methodology and principles of operation of the band-reject mechanism with stubs are generalized and can be applied to all uniplanar dual-band reject UWB antennas and even to some dual-layer designs. It can also easily be extended to multi-band reject antennas. The presented

dual band-reject mechanism with stubs was analyzed thoroughly. Furthermore, it can be used with other resonant or non-resonant (e.g., UWB) antenna structures in planar (e.g., rectangular, circular, elliptical) and/or volumetric configurations (e.g., rectangular, circular, elliptical, spherical, oval, cubiform), regardless of their feed mechanism.

The proposed design consists of linear sections only and is easy to replicate, fine-tune and fabricate. In addition, it is conformal, single-sided, has low gain at the rejected frequencies, low dispersion (flat group delay everywhere except at the rejected bands) that makes it useful in pulsed cognitive radio applications, while it improves the quality of UWB communication links in WLAN environments by increasing the S/N ratio at practically no additional fabrication cost.

REFERENCES

- [1] Fed. Commun. Comm, "First report and order, revision of part 15 of the commission's rule regarding ultra wideband transmission systems," FCC 02-48 Apr. 22, 2002.
- [2] *Part 11: Wireless LAN Medium Access Control (MAC) and Physical Layer (PHY) specifications: Physical Layer in the 5 GHz Band*, IEEE Std. 802.11a-1999(R2003), Jun. 12, 2003.
- [3] W. J. Lui, C. H. Cheng, and H. B. Zhu, "Improved frequency notched ultrawideband slot antenna using square ring resonator," *IEEE Trans. Antennas Propag.*, vol. 55, no. 9, pp. 2445–2450, 2007.
- [4] Y. J. Cho, K. K. Kim, D. H. Choi, S. S. Lee, and S. O. Park, "A miniature UWB planar monopole antenna with 5 GHz band rejection filter and the time domain characteristics," *IEEE Trans. Antennas Propag.*, vol. 54, no. 5, pp. 1453–1460, 2006.
- [5] T. Yang, W. A. Davis, and W. L. Stuzman, "Folded-notch dual band ultra-wideband antenna," in *Proc. IEEE APS Int. Symp.*, 2005, vol. 1B, pp. 520–523.
- [6] K. Bahadori and Y. Rahmat-Samii, "A miniaturized elliptic-card UWB antenna with WLAN band rejection for wireless communications," *IEEE Trans. Antennas Propag.*, vol. 55, no. 11, pp. 3326–3332, Nov. 2007.
- [7] H.-Y. Lai, Z.-Y. Lei, Y.-J. Xie, G.-L. Ning, and K. Yang, "UWB antenna with dual band rejection for WLAN/WiMAX bands using CSRRs," *Progr. Electromagn. Res. Lett.*, vol. 26, pp. 69–78, Aug. 2011.
- [8] C. R. Medeiros, J. R. Costa, and C. A. Fernandes, "Compact tapered slot UWB antenna with WLAN band rejection," *IEEE Antennas Wireless Propag. Lett.*, vol. 8, pp. 661–664, 2009.
- [9] K. S. Ryu and A. A. Kishk, "UWB antenna with single or dual band-notches for lower WLAN band upper WLAN band," *IEEE Trans. Antennas Propag.*, vol. 57, no. 12, pp. 3942–3950, Dec. 2009.
- [10] W. T. Li, X. W. Shi, and Y. Q. Hei, "Novel planar UWB monopole antenna with triple band-notched characteristics," *IEEE Antennas Wireless Propag. Lett.*, vol. 8, pp. 1094–1098, 2009.
- [11] D. E. Anagnostou, H. Kim, B. Kim, S. Nikolaou, J. Papapolymerou, and M. Tentzeris, "Dual band-notched ultra-wideband antenna for 802.11a LAN environments," in *Proc. IEEE APS Int. Symp.*, Honolulu, HI, Jun. 10–15, 2007, pp. 4621–4624.
- [12] R. N. Simons, *Coplanar Waveguide Circuits, Components, and Systems*. New York: Wiley, 2001, ch. 6.
- [13] W.-S. Lee, D.-Z. Kim, K.-J. Kim, and J.-W. Yu, "Wideband planar monopole antennas with dual band-notched characteristics," *IEEE Trans. Microwave Tech.*, vol. 54, no. 6, pp. 2800–2806, 2006.
- [14] D. M. Pozar, *Microwave Engineering*, 2nd ed. New York: Wiley, 1998.

Dual-Band Circularly Polarized Cavity-Backed Annular Slot Antenna for GPS Receiver

Wang-Ta Hsieh, Tze-Hsuan Chang, and Jean-Fu Kiang

Abstract—A circularly polarized (CP) cavity-backed annular slot antenna for GPS receiver is designed to operate in both the L1 and L2 bands of the Global Positioning System (GPS). The measured impedance bandwidths with VSWR less than 2 are 3.7% (1.19–1.235 GHz) and 1.2% (1.565–1.585 GHz), respectively, the measured 3 dB axial-ratio (AR) bandwidth are 0.9% (1.220–1.231 GHz) and 0.6% (1.572–1.581 GHz), respectively. A cavity is designed to render a unidirectional radiation pattern.

Index Terms—Annular slot, cavity backed, circular polarization, dual-band, GPS.

I. INTRODUCTION

Circular polarization (CP) is generally adopted in GPS and satellite communication due to Faraday rotation when signals pass through the ionosphere. GPS antennas with right-handed circular polarization (RHCP) are required to operate in both the L1 (1.575 GHz) and the L2 (1.227 GHz) bands. A circularly-polarized wave can be radiated by exciting two linearly polarized modes of the antenna, with equal amplitude, 90° phase difference, and orthogonal to each other in polarization. Such an excitation arrangement can be implemented using a single feed or dual feeds. A single-feed CP antenna is simple in structure, easy to fabricate, and requires no external feeding network [1]–[5]. With dual feeds, the input signals can be generated with a more complicated feeding structure via a hybrid or a Wilkinson power divider [6], [7].

Dual-band single-feed CP antennas have been realized in patch or slot forms [8]–[14]. In [8], four slits are engraved near the patch edges to elongate the current path, hence reducing the antenna size. Both TM_{10} and TM_{30} modes are excited to make a dual-band CP antenna, with a 1% of bandwidth within which the axial ratio (AR) is less than 3 dB. In [9], a dual-band CP patch antenna is designed by carving an asymmetric S-shaped slot to perturb the surface current, and the 3 dB AR bandwidths are 6.9% and 0.6%, respectively. In [10], a dual-band CP slot antenna is designed by attaching two deformed monopoles orthogonal to edges of a slot, and the 3 dB AR bandwidths are 9% and 11%, respectively. A dual-band CP slot antenna with dual senses has been achieved by loading two spirals at the opposite edges of a slot [11]. Patch antennas with stacked or multilayered structures have also been implemented for GPS applications in both the L1 and the L2 bands [12]–[14].

A dual-band GPS antenna is required to have, in both bands, a wide beamwidth facing the sky, a high front-to-back ratio to avoid interference from ground. In the proposed antenna, two concentric rectangular annular slots are carved on a printed circuit board (PCB) to create two

Manuscript received November 29, 2010; revised July 25, 2011; accepted September 06, 2011. Date of publication January 31, 2012; date of current version April 06, 2012. This work was sponsored by the National Science Council, Taiwan, ROC, under contract NSC 98-2221-E-002-050.

W.-T. Hsieh and J.-F. Kiang are with the Department of Electrical Engineering and the Graduate Institute of Communication Engineering, National Taiwan University, Taipei, Taiwan (e-mail: jfkiang@cc.ee.ntu.edu.tw).

T.-H. Chang is with the Foxconn, Taiwan.

Color versions of one or more of the figures in this communication are available online at <http://ieeexplore.ieee.org>.

Digital Object Identifier 10.1109/TAP.2012.2186229